

High-precision U-Pb age constraints on the Permian floral turnovers, paleoclimate change, and tectonics of the North China block

Qiong Wu¹, Jahandar Ramezani², Hua Zhang^{3,4*}, Jun Wang^{3,4}, Fangui Zeng⁵, Yichun Zhang^{3,4}, Feng Liu^{3,4}, Jun Chen⁶,

Yaofeng Cai^{3,4}, Zhangshuai Hou¹, Chao Liu⁵, Wan Yang⁷, Charles M. Henderson⁸ and Shu-zhong Shen^{1,4,9*}

¹State Key Laboratory for Mineral Deposits Research and School of Earth Sciences and Engineering, Nanjing University, Nanjing 210023, China

²Department of Earth, Atmospheric and Planetary Sciences, Massachusetts Institute of Technology, Cambridge, Massachusetts 02139, USA

³State Key Laboratory of Palaeobiology and Stratigraphy, Nanjing Institute of Geology and Palaeontology, Chinese Academy of Sciences, Nanjing 210008, China

⁴Center for Excellence in Life and Palaeoenvironment, Chinese Academy of Sciences, Nanjing 210023, China

⁵Department of Earth Science & Engineering, Taiyuan University of Technology, Taiyuan 030024, China

⁶State Key Laboratory of Isotope Geochemistry, Guangzhou Institute of Geochemistry, Chinese Academy of Sciences, Guangzhou 510640, China

⁷Geology and Geophysics Program, Missouri University of Science and Technology, Rolla, Missouri 65409, USA

⁸Department of Geoscience, University of Calgary, Calgary, AB T2N 1N4, Canada

⁹Key Laboratory of Continental Collision and Plateau Uplift, Institute of Tibetan Plateau Research and Center for Excellence in Tibetan Plateau Earth Sciences, Chinese Academy of Sciences, Beijing 100101, China

ABSTRACT

The Permian marine-terrestrial system of the North China block provides an exceptional window into the evolution of northern temperate ecosystems during the critical transition from icehouse to greenhouse following the late Paleozoic ice age (LPIA). Despite many studies on its rich hydrocarbon reserves and climate-sensitive fossil flora, uncertain temporal constraints and correlations have hampered a thorough understanding of the records of geologic, biologic, and climatic change from the North China block. We present a new chronostratigraphy based on high-precision U-Pb chemical abrasion–isotope dilution–thermal ionization mass spectrometry (CA-ID-TIMS) geochronology of tuffs from a near-complete latest Carboniferous–Permian succession in North China. The results indicate that the predominance of continental red beds, climate aridification, and the disappearance of coals and characteristic tropical flora were well under way during the Cisuralian (Early Permian) in the North China block, significantly earlier than previously thought. A nearly 20 m.y. hiatus spanning the early Kungurian to the mid-Guadalupian (or later) is revealed in the northern North China block to have close temporal and spatial associations with the closure and/or subduction of the Paleo-Asian Ocean and its related tectonic convergence. This long hiatus was concomitant with the prominent loss of the highly diverse and abundant Cathaysian floras and the widespread invasion of the monotonous Angaran floras under arid climate conditions in the North China block. Similarities in the floral and climate shift histories between Euramerica and North China suggest that aside from the regional tectonic controls and continental movement, extensive volcanism during the Cisuralian may have played a major role in the global warming and aridification in the aftermath of the LPIA.

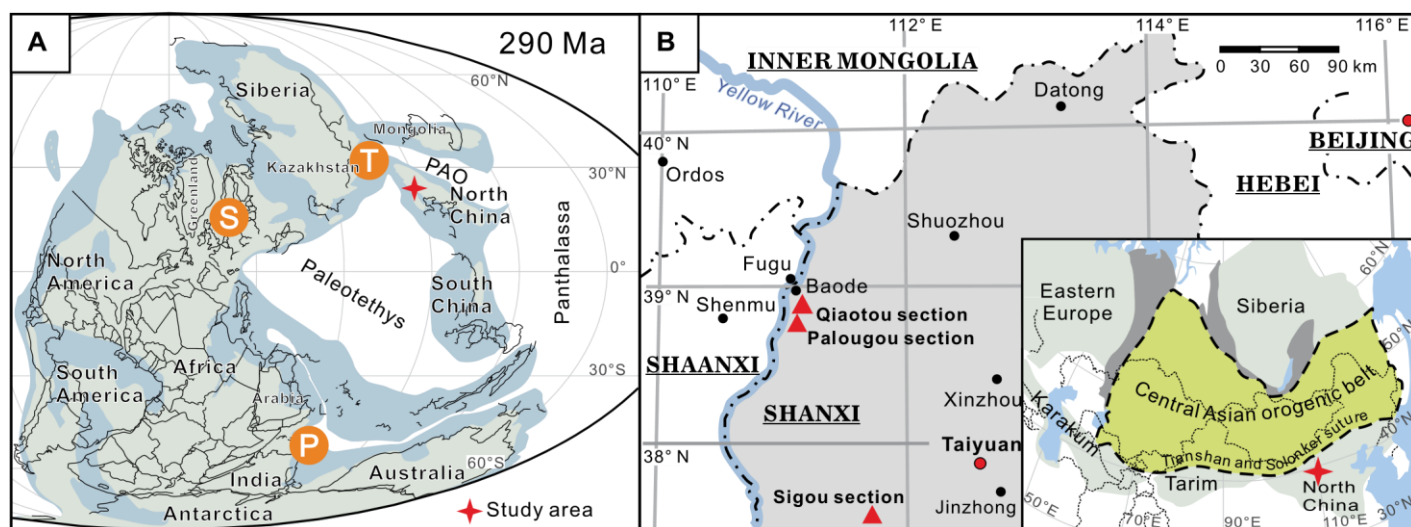
INTRODUCTION

The North China block occupied northerly tropical to subtropical paleolatitudes (Boucot et al., 2013), marginal to the Paleo-Asian Ocean (PAO), during the critical Cisuralian (298.9–273.0) transitions from an icehouse to a greenhouse world (Fig. 1). The late Carboniferous to Permian marine and marginal-marine to terrestrial sequences in North China preserve highly diverse and abundant plant fossils in addition to their significant economic hydrocarbon resources (Yang et al., 2005; Wang, 2010; Liu et al., 2015). These characteristics provide a unique opportunity to investigate the interactions among terrestrial biotic evolution, regional tectonics, and global climate change during a critical period of geologic history. However, poor constraints on age and correlation have hampered a deep understanding of those events in the North China block. In the absence of diagnostic marine fossils from key intervals, stratigraphic correlation within and beyond North China has relied on uncalibrated palynostratigraphy and phytostратigraphy (Wang, 2010; Liu et al., 2015) and magnetostratigraphy (Embleton et al., 1996). Detrital zircon geochronology by U-Pb *in situ* analyses from Permian volcanoclastic sandstones (e.g., Zhu et al., 2014;

*E-mails: szshen@nju.edu.cn; hzhang@nigpas.ac.cn

CITATION: Wu, Q., et al., 2021, High-precision U-Pb age constraints on the Permian floral turnovers, paleoclimate change, and tectonics of the North China block:

| GEOLOGY | Volume XX | Number XX | www.gsapubs.org



Geological Society of America

Figure 1. Location of study area. (A) Reconstruction of Cisuralian paleogeography (Boucot et al., 2013) showing the study area and major volcanic provinces. PAO—Paleo-Asian Ocean; P—Panjal Traps; S—Skagerrak-Centered large igneous province (LIP); T—Tarim LIP. (B) Loca-

tions of study sections in Shanxi Province, North China.

Yang et al., 2017) generally lacked the necessary precision or stratigraphic range to place reliable constraints on depositional ages.

We report high-precision U-Pb zircon geochronology by the chemical abrasion–isotope dilution–thermal ionization mass spectrometry (CA-ID-TIMS) method focused on bentonitic tuffs from the Permian succession in North China. The results necessitate fundamental revisions to the traditional Permian terrestrial depositional history and chronostratigraphy of the North China block and provide a new timeline and important insights for the history of continental collision, floral turnovers, and paleoclimate change as recorded in the North China block.

STRATIGRAPHY AND GEOLOGIC SETTING

Paleozoic epicontinental deposition in the North China block was interrupted by a long period of craton-wide non-deposition and/or erosion from the Late Ordovician to late Carboniferous (Yang et al., 2005). A late Carboniferous marine transgression led to the deposition of the Penchi Formation, overlain by the Carboniferous–Permian Taiyuan Formation, in shallow-marine and tidal-flat environments. The latter consists of alternating marine limestone and shale along with extensive coal seams that transition upward into lagoonal-swamp and shoreline deposits. The overlying Permian successions are predominated by fluvial-deltaic deposits with coal interbeds of the Shansi and Lower Shihhotse Formations, whereas the Upper Shihhotse Formation marks

a transition into mottled purple-red, fluvial and shallow-lacustrine mudstone, siltstone, and intercalated channel sandstone without coals (Yang et al., 2005). The overlying Sunjiagou Formation, which was deposited in a fluvial environment, is composed of typical red beds interbedded with stream channel-fill sandstone (Liu et al., 2015). Carboniferous–Permian basin evolution in North China was largely controlled by convergent tectonics during the closure of the PAO along the northern margin of the North China block (Zhu et al., 2014).

The age and regional correlation of the Penchi and Taiyuan Formations have been well constrained by fusuline and conodont fossils from their marine strata (see the Supplemental

Material¹⁾) as well as new U-Pb CA-ID-TIMS geochronology from the subsurface of southeastern North China (Yang et al., 2020). However, the correlation of the Permian succession above the Taiyuan Formation has long been a subject of debate. The Shansi and Lower Shihhotse Formations were roughly assigned to the Cisuralian, the Upper Shihhotse Formation to the Guadalupian (273.0–259.5 Ma), and the Sunjiagou Formation to the Lopingian (259.5–251.9 Ma) in the classic area of Shanxi Province in North China, based on fossil plant and palynological analyses (Wang, 2010; Liu et al., 2015).

Limited tuff zircon geochronology by *in situ* techniques previously resulted in U-Pb age estimates of 293.0 ± 2.5 Ma for the Shansi Formation (Yang et al., 2014), 290.1 ± 5.8 Ma for a northerly correlative of the Taiyuan and/or Shansi Formations (Cope et al., 2005), and 296 ± 4 Ma for a presumed correlative unit of the Lower and Upper Shihhotse Formations (Zhang et al., 2007). These data have been

unable to resolve outstanding Permian chronostratigraphic issues in North China (see the Supplemental Material for a complete review).

METHODS AND RESULTS

We collected 11 bentonitic tuff and tuffaceous mudstone samples from the Palougou, Qiaotou, and Sigou sections in Shanxi Province, northern North China (Fig. 1), for U-Pb geochronology by the CA-ID-TIMS method. These samples encompass the middle Taiyuan to basal Sunjiagou Formations. The weighted mean ²⁰⁶Pb/²³⁸U dates of the analyzed zircons along with a Bayesian interpolation algorithm are used to construct a statistically robust chronostratigraphic framework for the Permian succession of North China, from which the ages of lithostratigraphic boundaries, floral changes, and climate proxies can be extrapolated. Detailed descriptions of the stratigraphy, tuff samples, U-Pb analytical procedures, data reduction, age interpretation, reliability, and Bayesian modeling are provided in the Supplemental Material. The U-Pb

geochronological results are summarized in Table 1.

DISCUSSION

A set of five new weighted mean ²⁰⁶Pb/²³⁸U dates from bentonites of the Palougou section forms the basis of a Bayesian age-stratigraphic model, which for the first time provides a nearcomplete temporal calibration for the Permian system of North China (Fig. 2; Fig. S5 in the Supplemental Material). The Carboniferous-Permian boundary is precisely constrained at a major coal seam immediately below the dated tuff bed NC-3, based on the marine boundary calibration from the southern Ural Mountains (Russia) (Ramezani et al., 2007) and consistent with its biostratigraphic placement in the Taiyuan Formation (see the Supplemental Material). Results from the Qiaotou section provides a direct correlation of the major Asselian (298.9–293.5 Ma) coal seams (Shansi Formation) to the Palougou section (Figs. S1 and S5). The new chronostratigraphy assigns the interval

TABLE 1. SUMMARY OF CALCULATED U-Pb DATES AND THEIR UNCERTAINTIES														
Sample	Latitude		Longitude		Section	Formation	²⁰⁶ Pb/ ²³⁸ U age (Ma)	Error (2σ)*			MSWD†	n‡	N	
	(N)	(E)	(N)	(E)				X	Y	Z				
SG-18-D-05	37°40'06.61	111°56'45.05	0.29	N/A	N/A	16 N Sigou	261.75	0.12	0.32	0.49	0.96	4	6	
BD083019-2	38°45'45.12	111°05'58.49	280.98	0.11	0.15	0.34	260.10	0.10	0.32	0.37	0.96	4	6	
BD083019-3	38°45'45.12	111°05'58.49	280.98	0.11	0.15	0.34	260.10	0.10	0.32	0.37	0.96	4	6	
BD083019-4	38°45'45.12	111°05'58.49	280.98	0.11	0.15	0.34	260.10	0.10	0.32	0.37	0.96	4	6	
BD083019-5	38°45'45.12	111°05'58.49	280.98	0.11	0.15	0.34	260.10	0.10	0.32	0.37	0.96	4	6	
BD083019-6	38°45'45.12	111°05'58.49	280.98	0.11	0.15	0.34	260.10	0.10	0.32	0.37	0.96	4	6	
BD083019-7	38°45'45.12	111°05'58.49	280.98	0.11	0.15	0.34	260.10	0.10	0.32	0.37	0.96	4	6	
BD083019-8	38°45'45.12	111°05'58.49	280.98	0.11	0.15	0.34	260.10	0.10	0.32	0.37	0.96	4	6	
BD083019-9	38°45'45.12	111°05'58.49	280.98	0.11	0.15	0.34	260.10	0.10	0.32	0.37	0.96	4	6	
BD083019-10	38°45'45.12	111°05'58.49	280.98	0.11	0.15	0.34	260.10	0.10	0.32	0.37	0.96	4	6	
BD083019-11	38°45'45.12	111°05'58.49	280.98	0.11	0.15	0.34	260.10	0.10	0.32	0.37	0.96	4	6	
BD083019-12	38°45'45.12	111°05'58.49	280.98	0.11	0.15	0.34	260.10	0.10	0.32	0.37	0.96	4	6	
BD083019-13	38°45'45.12	111°05'58.49	280.98	0.11	0.15	0.34	260.10	0.10	0.32	0.37	0.96	4	6	
BD083019-14	38°45'45.12	111°05'58.49	280.98	0.11	0.15	0.34	260.10	0.10	0.32	0.37	0.96	4	6	
BD083019-15	38°45'45.12	111°05'58.49	280.98	0.11	0.15	0.34	260.10	0.10	0.32	0.37	0.96	4	6	
BD083019-16	38°45'45.12	111°05'58.49	280.98	0.11	0.15	0.34	260.10	0.10	0.32	0.37	0.96	4	6	
BD083019-17	38°45'45.12	111°05'58.49	280.98	0.11	0.15	0.34	260.10	0.10	0.32	0.37	0.96	4	6	
BD083019-18	38°45'45.12	111°05'58.49	280.98	0.11	0.15	0.34	260.10	0.10	0.32	0.37	0.96	4	6	
BD083019-19	38°45'45.12	111°05'58.49	280.98	0.11	0.15	0.34	260.10	0.10	0.32	0.37	0.96	4	6	
BD083019-20	38°45'45.12	111°05'58.49	280.98	0.11	0.15	0.34	260.10	0.10	0.32	0.37	0.96	4	6	
BD083019-21	38°45'45.12	111°05'58.49	280.98	0.11	0.15	0.34	260.10	0.10	0.32	0.37	0.96	4	6	
BD083019-22	38°45'45.12	111°05'58.49	280.98	0.11	0.15	0.34	260.10	0.10	0.32	0.37	0.96	4	6	
BD083019-23	38°45'45.12	111°05'58.49	280.98	0.11	0.15	0.34	260.10	0.10	0.32	0.37	0.96	4	6	
BD083019-24	38°45'45.12	111°05'58.49	280.98	0.11	0.15	0.34	260.10	0.10	0.32	0.37	0.96	4	6	
BD083019-25	38°45'45.12	111°05'58.49	280.98	0.11	0.15	0.34	260.10	0.10	0.32	0.37	0.96	4	6	
BD083019-26	38°45'45.12	111°05'58.49	280.98	0.11	0.15	0.34	260.10	0.10	0.32	0.37	0.96	4	6	
BD083019-27	38°45'45.12	111°05'58.49	280.98	0.11	0.15	0.34	260.10	0.10	0.32	0.37	0.96	4	6	
BD083019-28	38°45'45.12	111°05'58.49	280.98	0.11	0.15	0.34	260.10	0.10	0.32	0.37	0.96	4	6	
BD083019-29	38°45'45.12	111°05'58.49	280.98	0.11	0.15	0.34	260.10	0.10	0.32	0.37	0.96	4	6	
BD083019-30	38°45'45.12	111°05'58.49	280.98	0.11	0.15	0.34	260.10	0.10	0.32	0.37	0.96	4	6	
BD083019-31	38°45'45.12	111°05'58.49	280.98	0.11	0.15	0.34	260.10	0.10	0.32	0.37	0.96	4	6	
BD083019-32	38°45'45.12	111°05'58.49	280.98	0.11	0.15	0.34	260.10	0.10	0.32	0.37	0.96	4	6	
BD083019-33	38°45'45.12	111°05'58.49	280.98	0.11	0.15	0.34	260.10	0.10	0.32	0.37	0.96	4	6	
BD083019-34	38°45'45.12	111°05'58.49	280.98	0.11	0.15	0.34	260.10	0.10	0.32	0.37	0.96	4	6	
BD083019-35	38°45'45.12	111°05'58.49	280.98	0.11	0.15	0.34	260.10	0.10	0.32	0.37	0.96	4	6	
BD083019-36	38°45'45.12	111°05'58.49	280.98	0.11	0.15	0.34	260.10	0.10	0.32	0.37	0.96	4	6	
BD083019-37	38°45'45.12	111°05'58.49	280.98	0.11	0.15	0.34	260.10	0.10	0.32	0.37	0.96	4	6	
BD083019-38	38°45'45.12	111°05'58.49	280.98	0.11	0.15	0.34	260.10	0.10	0.32	0.37	0.96	4	6	
BD083019-39	38°45'45.12	111°05'58.49	280.98	0.11	0.15	0.34	260.10	0.10	0.32	0.37	0.96	4	6	
BD083019-40	38°45'45.12	111°05'58.49	280.98	0.11	0.15	0.34	260.10	0.10	0.32	0.37	0.96	4	6	
BD083019-41	38°45'45.12	111°05'58.49	280.98	0.11	0.15	0.34	260.10	0.10	0.32	0.37	0.96	4	6	
BD083019-42	38°45'45.12	111°05'58.49	280.98	0.11	0.15	0.34	260.10	0.10	0.32	0.37	0.96	4	6	
BD083019-43	38°45'45.12	111°05'58.49	280.98	0.11	0.15	0.34	260.10	0.10	0.32	0.37	0.96	4	6	
BD083019-44	38°45'45.12	111°05'58.49	280.98	0.11	0.15	0.34	260.10	0.10	0.32	0.37	0.96	4	6	
BD083019-45	38°45'45.12	111°05'58.49	280.98	0.11	0.15	0.34	260.10	0.10	0.32	0.37	0.96	4	6	
BD083019-46	38°45'45.12	111°05'58.49	280.98	0.11	0.15	0.34	260.10	0.10	0.32	0.37	0.96	4	6	
BD083019-47	38°45'45.12	111°05'58.49	280.98	0.11	0.15	0.34	260.10	0.10	0.32	0.37	0.96	4	6	
BD083019-48	38°45'45.12	111°05'58.49	280.98	0.11	0.15	0.34	260.10	0.10	0.32	0.37	0.96	4	6	
BD083019-49	38°45'45.12	111°05'58.49	280.98	0.11	0.15	0.34	260.10	0.10	0.32	0.37	0.96	4	6	
BD083019-50	38°45'45.12	111°05'58.49	280.98	0.11	0.15	0.34	260.10	0.10	0.32	0.37	0.96	4	6	
BD083019-51	38°45'45.12	111°05'58.49	280.98	0.11	0.15	0.34	260.10	0.10	0.32	0.37	0.96	4	6	
BD083019-52	38°45'45.12	111°05'58.49	280.98	0.11	0.15	0.34	260.10	0.10	0.32	0.37	0.96	4	6	
BD083019-53	38°45'45.12	111°05'58.49	280.98	0.11	0.15	0.34	260.10	0.10	0.32	0.37	0.96	4	6	
BD083019-54	38°45'45.12	111°05'58.49	280.98	0.11	0.15	0.34	260.10	0.10	0.32	0.37	0.96	4	6	
BD083019-55	38°45'45.12	111°05'58.49	280.98	0.11	0.15	0.34	260.10	0.10	0.32	0.37	0.96	4	6	
BD083019-56	38°45'45.12	111°05'58.49	280.98	0.11	0.15	0.34	260.10	0.10	0.32	0.37	0.96	4	6	
BD083019-57	38°45'45.12	111°05'58.49	280.98	0.11	0.15	0.34	260.10	0.10	0.32	0.37	0.96	4	6	
BD083019-58	38°45'45.12	111°05'58.49	280.98	0.11	0.15	0.34	260.10	0.10	0.32	0.37	0.96	4	6	
BD083019-59	38°45'45.12	111°05'58.49	280.98	0.11	0.15	0.34	260.10	0.10	0.32	0.37	0.96	4	6	
BD083019-60	38°45'45.12	111°05'58.49	280.98	0.11	0.15	0.34	260.10	0.10	0.32	0.37	0.96	4	6	
BD083019-61	38°45'45.12	111°05'58.49	280.98	0.11	0.15	0.34	260.10	0.10	0.32	0.37	0.96	4	6	
BD083019-62	38°45'45.12	111°05'58.49	280.98	0.11	0.15	0.34	260.10	0.10	0.32	0.37	0.96	4	6	
BD083019-63	38°45'45.12	111°05'58.49	280.98	0.11	0.15	0.34	260.10	0.10	0.32	0.37	0.96	4	6	
BD083019-64	38°45'45.12	111°05'58.49	280.98	0.11	0.15	0.34	260.10	0.10	0.32	0.37	0.96	4	6	
BD083019-65	38°45'45.12	111°05'58.49	280.98	0.11	0.15	0.34	260.10	0.10	0.32	0.37	0.96	4	6	
BD083019-66	38°45'45.12	111°05'58.49	280.98	0.11	0.15	0.34	260.10	0.10	0.32	0.37	0.96	4	6	
BD083019-67	38°45'45.12	111°05'58.49	280.98	0.11	0.15	0.34	260.10	0.10	0.32	0.37	0.96	4	6	
BD083019-68	38°45'45.12	111°05'58.49	280.98	0.11	0.15	0.34	260.10	0.10	0.32	0.37	0.96	4	6	
BD083019-69	38°45'45.12	111°05'58.49	280.98	0.11	0.15	0.34	260.10	0.10	0.32	0.37	0.96	4	6	
BD083019-70	38°45'45.12	111°05'58.49	280.98	0.11	0.15	0.34	260.10	0.10	0.32	0.37	0.96	4	6	
BD083019-71	38°45'45.12	111°05'58.49	280.98	0.11	0.15	0.34	260.10	0.10	0.32	0.37	0.96	4	6	
BD083019-72	38°45'45.12	111°05'58.49	280.98	0.11	0.15	0.34	260.10	0.10	0.32	0.37	0.96	4	6	
BD083019-73	38°45'45.12	111°05'58.49	280.98	0.11	0.15	0.34	260.10	0.10	0.32	0.37	0.96	4	6	
BD083019-74	38°45'45.12	111°05'58.49	280.98	0.11	0.15	0.34	260.10	0.10	0.32	0.37	0.96	4	6	
BD083019-75	38°45'45.12	111°05'58.49	280.98	0.11	0.15	0.34	260.10	0.10	0.32	0.37	0.96	4	6	
BD083019-76	38°45'45.12	111°05'58.49	280.98	0.11	0.15	0.34	260.10	0.10	0.32	0.37	0.96	4	6	
BD083019-77	38°45'45.12	111°05'58.49	280.98	0.11	0.15	0.34	260.10	0.10	0.32	0.37	0.96	4	6	
BD083019-78	38°45'45.12	111°05'58.49	280.98	0.11	0.15	0.34	260.10	0.10	0.32	0.37	0.96	4	6	
BD083019-79	38°45'45.12	111°05'58.49	280.98	0.11	0.15	0.34	260.10	0.10	0.32	0.37	0.96	4	6	
BD083019-80	38°45'45.12	111°05'58.49	280.98	0.11	0.15	0.34	260.10	0.10	0.32	0.37	0.96	4	6	
BD083019-81	38°45'45.12	111°05'58.49	280.98	0.11	0.15	0.34	260.10	0.10	0.32	0.37	0.96	4	6	
BD083019-82	38°45'45.12	111°05'58.49	280.98	0.11	0.15	0.34	260.10	0.10	0.32	0.37				

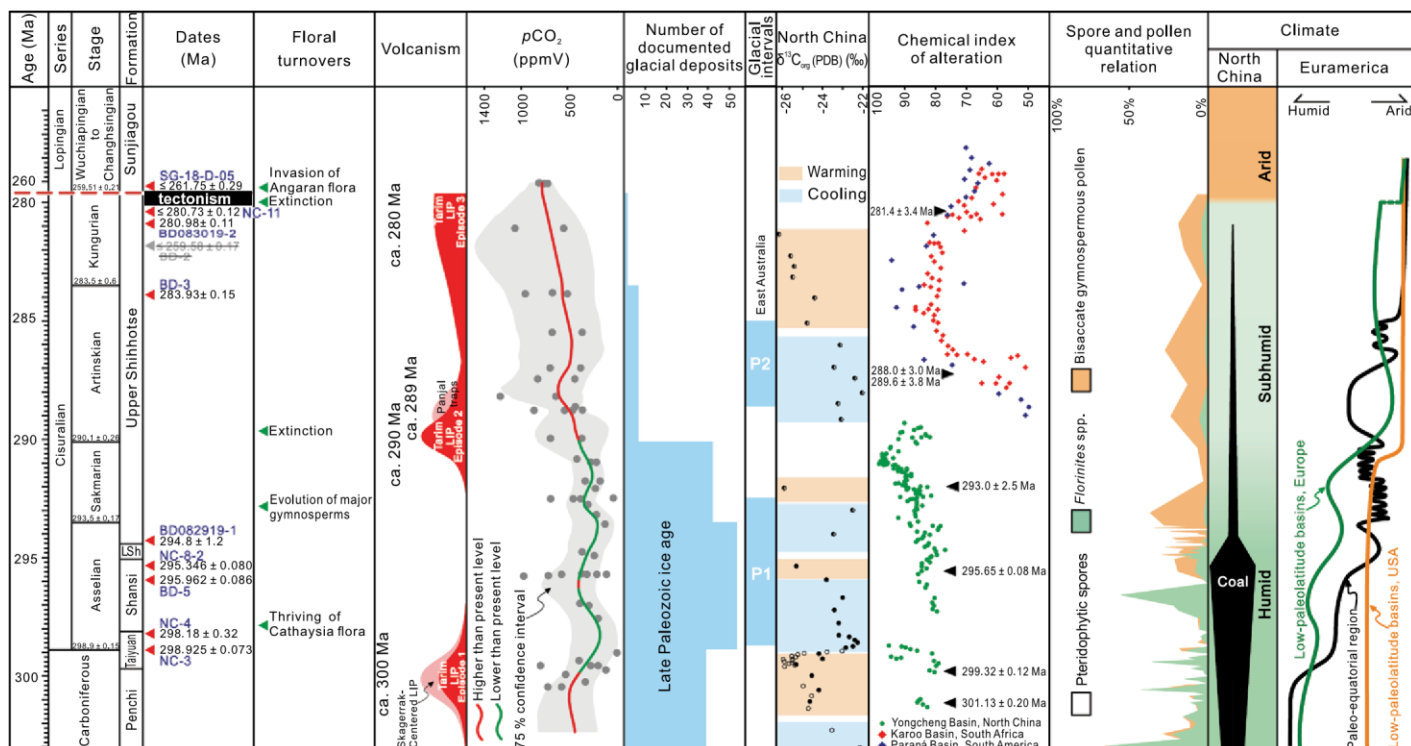


Figure 2. Compilation of Permian global events in parallel with Earth system changes in the North China block. Red dashed line represents the unconformity from the late Cisuralian to Guadalupian (ca. 280–260 Ma) between the Upper Shihhotse and Sunjiagou Formations. LSh—Lower Shihhotse. Red triangles indicate dated samples. Floral turnover patterns in the North China block are modified from Wang (2010) and Stevens et al. (2011). Main episodes of Panjal Traps, Skagerrak-Centered large igneous province (LIP) and Tarim LIP volcanism are after Shellenutt (2018), Torsvik et al. (2008), and Xu et al. (2014), respectively. Global atmospheric $p\text{CO}_2$ curve is after Richey et al. (2020). Documented glacial deposits are after Soreghan et al. (2019). Glacial intervals in Australia are after Garbelli et al. (2019). $\delta^{13}\text{C}_{\text{org}}$ (PDB—Peedee belemnite) of coals in North China is after Zhang et al. (1999). Chemical index of alteration and ages marked as black triangles are after Yang et al. (2014, 2020) and references therein. Quantitative relation of Permian spore and pollen in the North China block is after Liu et al. (2015). Cisuralian Euramerican climate transitions are after Tabor and Poulsen (2008).

Geological Society of America

Figure 3. Carboniferous–Permian paleogeography including terrestrial climate-sensitive indicators and illustrating expanded arid zones in middle to low paleolatitudes, modified after Tabor and Poulsen (2008) and Boucot et al. (2013).

evaluation of existing *in situ* U–Pb detrital zircon geochronology substantiates a similar hiatus in the Permian successions of North China, although its duration may vary as a function of proximity to the collisional zone in the north of the North China block (Fig. S3; Table S2). Paleosols in the upper half of the Upper Shihhotse Formation may account for minor hiatuses before the single major

unconformity associated with the basal channel

Downloaded from gsapubs.org

(conglomeratic) sandstone of the overlying

Sunjiagou Formation (Fig. S2). An analogous

Downloaded from gsapubs.org

unconformity has also been reported from

correlative Permian successions in eastern

Xinjiang (Yang et al., 2010) and Inner

Mongolia (Tang and Yan, 1993). These areas

Downloaded from gsapubs.org

constituted the southern margins of the PAO,

the middle segment of which underwent

Downloaded from gsapubs.org

tectonic convergence (uplift and erosion)

associated with subduction generating arc-

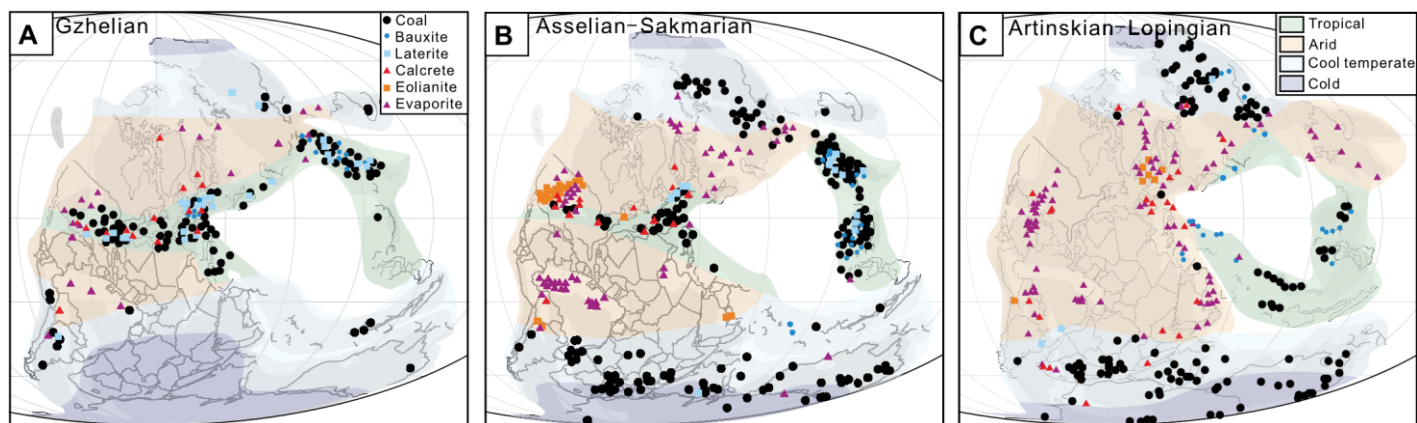
continent and retroarc fold-thrust deformation

or ocean closure leading to continental collision

Downloaded from gsapubs.org

(ca. 280–265 Ma: Zhao et al., 2018; Xiao et al.

2018).



A highly diverse Cathaysian flora and

extensive coal deposits preserved in the

Downloaded from gsapubs.org

Taiyuan and Shansi Formations indicate a

humid climate (Wang, 2010). The climate

Downloaded from gsapubs.org

became more arid from the late Asselian with

the increase of xerophytic plants and decrease

Downloaded from gsapubs.org

of coal deposits in the upper Shansi Formation

(Liu et al., 2015). The early main groups of

Downloaded from
http://pubs.geoscienceworld.org/

gymnosperms (e.g., early ginkgoaleans and

conifers) evolved afterward (Fig. 2; Wang,

2010). A notable change to a more arid

condition occurs across the major unconformity,

which separates the upper Upper Shihhotse

Formation subhumid paleosols containing

abundant flora from overlying Sunjiagou

Formation aeolian sandstone, carbonate

breccias, and gypsum with few plant fossils.

Aridification trends and analogous fossil-poor

Downloaded from gsapubs.org

red beds have also been recorded in middle to

low paleolatitudes during the Cisuralian to

Downloaded from gsapubs.org

Guadalupian, concomitant with deglaciation of

the late Paleozoic ice age (LPIA) and surge of

Downloaded from gsapubs.org

atmospheric CO₂ (Tabor and Poulsen, 2008;

Boucot et al., 2013; Schneider et al., 2019;

Downloaded from gsapubs.org

Soreghan et al.,

2019; Richey et al., 2020), except for Tethyan archipelagos where the ocean may have modulated climate (Figs. 2 and 3).

Northward continental drift into a subtropical or temperate arid climatic zone (Rees et al., 1999; Tabor and Poulsen, 2008) and/or a regional rain-shadow effect caused by orographic uplift associated with tectonic convergence (Cope et al., 2005) may have contributed to the late Asselian to Guadalupian aridification in the North China block. However, these regional effects do not explain a global-scale climate transition at this time. An increase in atmospheric CO₂ has long been considered the major driving force for the demise of the LPIA and subsequent global aridification, presumably due to elevated surface temperature and evaporation, which thus reduced soil moisture and the source of continental convective precipitation (Poulsen et al., 2007; Peyser and Poulsen, 2008). The surge in atmospheric CO₂ was probably related to extensive large igneous province (LIP) volcanism during the Cisuralian (e.g., Skagerrak-Centered LIP, Panjal Traps, Tarim LIP; Torsvik et al., 2008; Xu et al., 2014; Shellnutt, 2018; Fig. 1A), as suggested by the coincidence between LIPs and *p*CO₂ excursions (Fig. 2). The moderate increases of *p*CO₂ in between may have been associated with widespread wildfires (Yan et al., 2016). Furthermore, the warming phases associated with high *p*CO₂ were indicated by low δ¹³C_{org} values from Permo-Carboniferous coals in North China (Zhang et al., 1999), significant retreat of the LPIA (Soreghan et al., 2019), stronger terrestrial chemical weathering (Yang et al., 2014, 2020, and references therein), and interglacial intervals in Australia (Garbelli et al., 2019). Thus, frequent and extensive volcanism during the Cisuralian may have been responsible for reducing effects of the LPIA and global aridification under such CO₂-forced climate conditions.

Our new geochronology questions that scenario and instead indicates a temporal coincidence with the convergent tectonics of the PAO and the third phase of the Tarim LIP during the Kungurian (Xu et al., 2014). Both convergent tectonics and extensive volcanism may have profoundly influenced the local environments and climate, which in turn led to floral extinction at the top of the Upper Shihhotse Formation and possibly the Olson's gap of tetrapods from the late Cisuralian to the middle Guadalupian (Lucas, 2018). Progressive contraction (closure) of the central to eastern segment of the PAO during the Permian (to Early Triassic) (Eizenhöfer and Zhao, 2018) provided a pathway for the widespread invasion of Angaran flora to the North China block, as recorded in the lower Sunjiagou Formation (Wang, 2010). We interpret the abrupt floral disappearances at the top of the Upper Shihhotse Formation as an extinction event, but further work is needed to rule out the possibility that it is an artifact of stratigraphic truncation associated with the sub-Sunjiagou unconformity.

CONCLUSIONS

New high-precision U-Pb geochronology necessitates major revisions to the temporal framework for the Permian terrestrial system in North China. The Upper Shihhotse Formation spans the latest Asselian to the early Kungurian, as opposed to its previous Wordian to Wuchiapingian age assignments. A major depositional gap during the late Cisuralian to Guadalupian in the northern North China block may have been caused by convergent tectonics associated with the closure and/or subduction of the PAO. The great loss of highly diverse and abundant Cathaysian floras and the widespread invasion of the Angaran floras under arid climate conditions in the North China block happened during the late Cisuralian to Guadalupian, but its exact timing is uncertain due to the long hiatus. The Cisuralian global aridification may have been

The major floral disappearances in the topmost Upper Shihhotse Formation had previously been attributed to the late Capitanian Emeishan LIP (Bond et al., 2010; Stevens et al., 2011). associated with extensive LIP volcanism and the rise of atmospheric CO₂ in the waning stages of the LPIA.

ACKNOWLEDGMENTS

Mark Schmitz and Vladimir Davydov joined in an earlier field trip to North China. This research is supported by the Strategic Priority Research Programs of the Chinese Academy of Sciences (grants XDB18000000 and XDB26000000). Wan Yang is partially supported by the U.S. National Science Foundation (grant EAR 1714749). We thank Isabella Bennett for expeditious zircon separation at the Massachusetts Institute of Technology. We thank anonymous reviewers for their comments that improved the manuscript.

REFERENCES CITED

- Bond, D.G., Hilton, J., Wignall, P.B., Ali, J.R., Stevens, L.G., Sun, Y.D., and Lai, X.L., 2010, The Middle Permian (Capitanian) mass extinction on land and in the oceans: *Earth-Science Reviews*, v. 102, p. 100–116, <https://doi.org/10.1016/j.earscirev.2010.07.004>.
- Boucot, A.J., Chen, X., Scotese, C.R., and Morley, R.J., 2013, Phanerozoic Paleoclimate: An Atlas of Lithologic Indicators of Climate: SEPM (Society for Sedimentary Geology) Concepts in Sedimentology and Paleontology 11, 478 p., <https://doi.org/10.2110/sepmcsp.11>.
- Cope, T., Ritts, B.D., Darby, B.J., Fildani, A., and Graham, S.A., 2005, Late Paleozoic sedimentation on the northern margin of the North China block: Implications for regional tectonics and climate change: *International Geology Review*, v. 47, p. 270–296, <https://doi.org/10.2747/0020-6814.47.3.270>.
- Eizenhöfer, P.R., and Zhao, G.C., 2018, Solonker Suture in East Asia and its bearing on the final closure of the eastern segment of the Palaeo-Asian Ocean: *Earth-Science Reviews*, v. 186, p. 153–172, <https://doi.org/10.1016/j.earscirev.2017.09.010>.
- Embleton, B.J.J., McElhinny, M.W., Ma, X.H., Zhang, Z.K., and Li, Z.X., 1996, Permo-Triassic magnetostratigraphy in China: The type section near Taiyuan, Shanxi Province, North China: *Geophysical Journal International*, v. 126, p. 382–388, <https://doi.org/10.1111/j.1365-246X.1996.tb05298.x>.
- Garbelli, C., Shen, S.Z., Immenhauser, A., Brand, U., Buhl, D., Wang, W.Q., Zhang, H., and Shi, G.R., 2019, Timing of Early and Middle Permian deglaciation of the southern hemisphere: Brachiopod-based $^{87}\text{Sr}/^{86}\text{Sr}$ calibration: *Earth and Planetary Science Letters*, v. 516, p. 122–135, <https://doi.org/10.1016/j.epsl.2019.03.039>.
- Hounsflow, M.W., and Balabanov, Y.P., 2018, A geomagnetic polarity timescale for the Permian, calibrated to stage boundaries, in Lucas, S.G., and Shen, S.Z., eds., *The Permian Timescale: Geological Society [London] Special Publication 450*, p. 61–103, <https://doi.org/10.1144/SP450.8>.
- Liu, F., Zhu, H.C., and Ouyang, S., 2015, Late Pennsylvanian to Wuchiapingian palynostratigraphy of the Baode section in the Ordos Basin, North China: *Journal of Asian Earth Sciences*, v. 111, p. 528–552, <https://doi.org/10.1016/j.jseaes.2015.06.013>.
- Lucas, S.G., 2018, Permian tetrapod biochronology, correlation and evolutionary events, in Lucas, S.G., and Shen, S.Z., eds., *The Permian Timescale: Geological Society [London] Special Publication 450*, p. 405–444, <https://doi.org/10.1144/SP450.12>.
- Peyser, C.E., and Poulsen, C.J., 2008, Controls on Permo-Carboniferous precipitation over tropical Pangaea: A GCM sensitivity study: *Palaeogeography, Palaeoclimatology, Palaeoecology*, v. 268, p. 181–192, <https://doi.org/10.1016/j.palaeo.2008.03.048>.
- Poulsen, C.J., Pollard, D., Montañez, I.P., and Rowley, D., 2007, Late Paleozoic tropical climate response to Gondwanan deglaciation: *Geology*, v. 35, p. 771–774, <https://doi.org/10.1130/G23841A.1>.
- Ramezani, J., Schmitz, M.D., Davydov, V.I., Bowring, S.A., Snyder, W.S., and Northrup, C.J., 2007, High-precision U-Pb zircon age constraints on the Carboniferous-Permian boundary in the southern Urals stratotype: *Earth and Planetary Science Letters*, v. 256, p. 244–257, <https://doi.org/10.1016/j.epsl.2007.01.032>.
- Rees, P.M., Gibbs, M.T., Ziegler, A.M., Kutzbach, J.E., and Behling, P.J., 1999, Permian climates: Evaluating model predictions using global paleobotanical data: *Geology*, v. 27, p. 891–894, [https://doi.org/10.1130/0091-7613\(1999\)027<891:PCEMPU>2.3.CO;2](https://doi.org/10.1130/0091-7613(1999)027<891:PCEMPU>2.3.CO;2).
- Richey, J.D., Montañez, I.P., Goddérís, Y., Looy, C.V., Griffiths, N.P., and DiMichele, W.A., 2020, Influence of temporally varying weatherability on CO₂ climate coupling and ecosystem change in the late Paleozoic: *Climate of the Past*, v. 16, p. 1759–1775, <https://doi.org/10.5194/cp-16-1759-2020>.
- Schneider, J.W., et al., 2019, Late Paleozoic–early Mesozoic continental biostratigraphy—Links to the Standard Global Chronostratigraphic Scale: *Palaeoworld*, v. 29, p. 186–238, <https://doi.org/10.1016/j.palwor.2019.09.001>.
- Shellnutt, J.G., 2018, The Panjal Traps, in Sensarma, S., and Storey, B.C., eds., *Large Igneous Provinces from Gondwana and Adjacent Regions: Geological Society [London] Special Publication 463*, p. 59–86, <https://doi.org/10.1144/SP463.4>.
- Soreghan, G.S., Soreghan, M.J., and Heavens, N.G., 2019, Explosive volcanism as a key driver of the late Paleozoic ice age: *Geology*, v. 47, p. 600–604, <https://doi.org/10.1130/G46349.1>.
- Stevens, L.G., Hilton, J., Bond, D.P., Glasspool, I.J., and Jardine, P.E., 2011, Radiation and extinction patterns in Permian floras from North China as indicators for environmental and climate change: *Journal of the Geological Society*, v. 168, p. 607–619, <https://doi.org/10.1144/0016-76492010042>.
- Tabor, N.J., and Poulsen, C.J., 2008, Palaeoclimate across the Late Pennsylvanian–Early Permian tropical palaeolatitudes: A review of climate indicators, their distribution, and relation to palaeophysiographic climate factors: *Palaeogeography, Palaeoclimatology, Palaeoecology*, v. 268, p. 293–310, <https://doi.org/10.1016/j.palaeo.2008.03.052>.
- Tang, K.D., and Yan, Z.Y., 1993, Regional metamorphism and tectonic evolution of the Inner Mongolian suture zone: *Journal of Metamorphic Geology*, v. 11, p. 511–522, <https://doi.org/10.1111/j.1525-1314.1993.tb00168.x>.
- Torsvik, T.H., Smethurst, M.A., Burke, K., and Steinberger, B., 2008, Long term stability in deep mantle structure: Evidence from the ~300 Ma Skagerrak-Centered Large Igneous Province (the SCLIP): *Earth and Planetary Science Letters*, v. 267, p. 444–452, <https://doi.org/10.1016/j.epsl.2007.12.004>.
- Wang, J., 2010, Late Paleozoic macrofloral assemblages from Weibei Coalfield, with reference to vegetational change through the Late Paleozoic Ice-age in the North China Block: *International Journal of Coal Geology*, v. 83, p. 292–317, <https://doi.org/10.1016/j.coal.2009.10.007>.
- Xiao, W.J., Windley, B.F., Han, C.M., Liu, W., Wan, B., Zhang, J.E., Ao, S.J., Zhang, Z.Y., and Song, D.F., 2018, Late Paleozoic to early Triassic multiple roll-back and oroclinal bending of the Mongolia collage in Central

- Asia: *Earth-Science Reviews*, v. 186, p. 94–128, <https://doi.org/10.1016/j.earscirev.2017.09.020>.
- Xu, Y.G., Wei, X., Luo, Z.Y., Liu, H.Q., and Cao, J., 2014, The Early Permian Tarim Large Igneous Province: Main characteristics and a plume incubation model: *Lithos*, v. 204, p. 20–35, <https://doi.org/10.1016/j.lithos.2014.02.015>.
- Yan, M.X., Wan, M.L., He, X.Z., Hou, X.D., and Wang, J., 2016, First report of Cisuralian (early Permian) charcoal layers within a coal bed from Baode, North China with reference to global wildfire distribution: *Palaeogeography, Palaeoclimatology, Palaeoecology*, v. 459, p. 394–408, <https://doi.org/10.1016/j.palaeo.2016.07.031>.
- Yang, D.B., Yang, H.T., Shi, J.P., Xu, W.L., and Wang, F., 2017, Sedimentary response to the paleogeographic and tectonic evolution of the southern North China Craton during the late Paleozoic and Mesozoic: *Gondwana Research*, v. 49, p. 278–295, <https://doi.org/10.1016/j.gr.2017.06.009>.
- Yang, J.H., Cawood, P.A., Du, Y.S., Feng, B., and Yan, J.X., 2014, Global continental weathering trends across the Early Permian glacial to postglacial transition: Correlating high- and low-paleolatitude sedimentary records: *Geology*, v. 42, p. 835–838, <https://doi.org/10.1130/G35892.1>.
- Yang, J.H., Cawood, P.A., Montañez, I.P., Condon, D.J., Du, Y.S., Yan, J.X., Yan, S.Q., and Yuan, D.X., 2020, Enhanced continental weathering and large igneous province induced climate warming at the Permo-Carboniferous transition: *Earth and Planetary Science Letters*, v. 534, 116074, <https://doi.org/10.1016/j.epsl.2020.116074>.
- Yang, W., Feng, Q., Liu, Y.Q., Tabor, N., Miggins, D., Crowley, J.L., Lin, J.Y., and Thomas, S., 2010, Depositional environments and cyclo- and chronostratigraphy of uppermost Carboniferous–Lower Triassic fluvial-lacustrine deposits, southern Bogda Mountains, NW China—A terrestrial paleoclimatic record of mid-latitude NE Pangea: *Global and Planetary Change*, v. 73, p. 15–113, <https://doi.org/10.1016/j.gloplacha.2010.03.008>.
- Yang, Y.T., Li, W., and Ma, L., 2005, Tectonic and stratigraphic controls of hydrocarbon systems in the Ordos basin: A multicycle cratonic basin in central China: *American Association of Petroleum Geologists Bulletin*, v. 89, p. 255–269, <https://doi.org/10.1306/10070404027>.
- Zhang, H., Shen, G.L., and He, Z.L., 1999, A carbon isotopic stratigraphic pattern of the Late Palaeozoic coals in the North China Platform and its palaeoclimatic implications: *Acta Geologica Sinica*, v. 73, p. 111–119, <https://doi.org/10.1111/j.1755-6724.1999.tb00817.x>.
- Zhang, S.H., Zhao, Y., Song, B., and Yang, Y.H., 2007, Zircon SHRIMP U-Pb and in-situ Lu-Hf isotope analyses of a tuff from Western Beijing: Evidence for missing Late Paleozoic arc volcano eruptions at the northern margin of the North China block: *Gondwana Research*, v. 12, p. 157–165, <https://doi.org/10.1016/j.gr.2006.08.001>.
- Zhao, G.C., Wang, Y.J., Huang, B.C., Dong, Y.P., Li, S.Z., Zhang, G.W., and Yu, S., 2018, Geological reconstructions of the East Asian blocks: From the breakup of Rodinia to the assembly of Pangea: *Earth-Science Reviews*, v. 186, p. 262–286, <https://doi.org/10.1016/j.earscirev.2018.10.003>.
- Zhu, X.Q., Zhu, W.B., Ge, R.F., and Wang, X., 2014, Late Paleozoic provenance shift in the southcentral North China Craton: Implications for tectonic evolution and crustal growth: *Gondwana Research*, v. 25, p. 383–400, <https://doi.org/10.1016/j.gr.2013.04.009>.
- Zhu, Z.C., et al., 2019, Altered fluvial patterns in North China indicate rapid climate change linked to the Permian-Triassic mass extinction: *Scientific Reports*, v. 9, 16818, <https://doi.org/10.1038/s41598-019-53321-z>.

Printed in USA